International Journal of Energy Production and Management
Vol. 8, No. 4, December, 2023, pp. 211-218
Journal homepage: http://iieta.org/journals/ijepm

# Evaluation of 15-m-Height Solar Chimney Model Integrated with TES under Tropical Climate

Hussain H. Al-Kayiem[1*], Hasanain A. Abdul Wahhab[2], Iylia E.A. Jamil[3], Mohamed M. Mohamed[3], Ibrahim M. Mohamed[3]

[1] Air Conditioning and Refrigeration Techniques Engineering Department, Hilla University College, Babylon 51001, Iraq
[2] Training and Workshop Center, University of Technology, Baghdad 35050, Iraq
[3] Mechanical Engineering Department, Universiti Teknologi PETRONAS, Seri Iskandar 32610, Malaysia

Corresponding Author Email: prof.hussain@acaress.org



https://doi.org/10.18280/ijepm.080402

**Received:** 11 October 2023
**Revised:** 3 November 2023
**Accepted:** 1 December 2023
**Available online:** 29 December 2023

***Keywords:***
*experimental solar chimney, solar updraft power, sensible TES, solar chimney power plant*

**ABSTRACT**

The present study examines a solar chimney power generation model under tropical conditions, with a focus on the impact of ground absorber dimensions on system efficacy. An experimental and numerical analysis was conducted using a 15-meter-high solar chimney, where the ground was transformed into a sensible thermal energy storage system through the application of black-painted pebbles. Three configurations were assessed to determine system performance: Case-1 and Case-2, featuring collector diameters of 4.9 m and 6.6 m respectively, and Case-3, which introduces an innovative design extending the diameter of the sensible thermal energy storage (TES) by 2.0 m beyond the collector's canopy. Performance was gauged using a metric defined by the product of mass flow rate and temperature increase of the air. Numerical models were validated against experimental outcomes, with results showing a satisfactory correlation. It was found that the performance metric in Case-2 doubled, while in Case-3, it tripled relative to Case-1. The enhancement in performance in Case-3 was further evidenced by a 30.4% increase in air velocity at the chimney base over Case-2, and a 36.7% increase over Case-1, highlighting the efficacy of the extended sensible TES. These findings suggest that enlarging the TES area beyond the collector's canopy can significantly improve solar chimney performance, potentially enabling a reduction in construction scale and a concurrent decrease in electricity production costs. This approach represents a promising avenue for addressing the dual challenges of structural height and efficiency that currently hamper the feasibility of solar chimney power generation on an industrial scale.

## 1. INTRODUCTION

The integration of renewable energy resources into the global power generation portfolio is imperative for mitigating carbon emissions and fostering environmental sustainability. Solar chimney power plants (SCPPs) are $CO_2$-neutral systems that leverage solar radiation to generate electricity without chemical reactions, thus contributing to the stabilization of supply-demand dynamics and the safeguarding of the global environment.

The pioneering SCPP prototype was constructed in Manzanares, Spain, in 1982, consisting of a 244-meter-diameter collector, a 196-meter-tall chimney, and a turbine, achieving a 50-kW output with an air velocity of 15 m/s at the chimney's base. Subsequent studies sought to address the inherent low efficiency and the challenges associated with the scale of the collector and chimney through a plethora of experimental, computational, and mathematical approaches. Comprehensive reviews have synthesized advancements in SCPP technology, as in Chikere et al. [1], Al-Kayiem and Chikere [2], Kasaeian et al. [3], and more recent analyses of hybrid systems by Ahmed et al. [4], and evaluations of SCPP concepts and performance by Cuce et al. [5].

At Universiti Teknologi PETRONAS (UTP), a scaled-down SCPP model with a 6.0-meter-diameter collector and a 6.3-meter chimney has been the subject of extensive research. Investigations into collector geometry's impact on performance, as detailed by Al-Azawiey et al. [6], have demonstrated that larger collector areas significantly enhance air velocity within the chimney. Modifications to the SC model, including adjustable canopy height, were reported by Al-Azawiey et al. [7] to optimize efficiency across various collector inlet heights, with a 0.05-meter inlet height showing superior performance.

Further experimental studies include the 8-meter chimney and 10-meter diameter collector model by Zhou et al. [8], which registered a maximum updraft velocity of 2.13 m/s in Wuhan City, China. In Iran, an SCPP model with a 12-meter chimney and a 10-meter collector diameter was evaluated by Kasaeian et al. [9], focusing on air inversion phenomena and

temperature variations within the system. A notable outlier in reported velocities is the claim of a 12.2 m/s air velocity at the chimney base by Lal et al. [10] from a model in Rajasthan Technical University Kota, India, a finding that stands in contrast to established literature. Rao [11] analyzed a stack shaft in a building, indicating that increased chimney heights correlate with more reliable hydrothermal process measurements.

Considering these findings, the scale of the SC model at UTP was increased to a 15-meter chimney to enhance the reliability of velocity and temperature measurements. This paper aims to present a comprehensive evaluation of the scaled-up system through experimental and numerical simulations under tropical conditions. The assessment spans various solar irradiances and three distinct configurations of the collector and sensible thermal energy storage (TES), denoted as Case-1 (4.9 m collector diameter), Case-2 (6.6 m collector diameter), and a novel Case-3, incorporating an extended diameter of 6.6 + 2 m for the sensible TES.

## 2. EXPERIMENTAL METHODOLOGY

A 6.3-m-height SC experimental model was modified to an updated version of a 15-m-height SC model to acquire experimental measurement data. The collector was also modified in terms of size and absorbing ground materials. The experimental setup is in the solar research site of UTP at 4° 23' 6.59" N 100° 58' 28.19" E.

### 2.1 Description of the experimental model

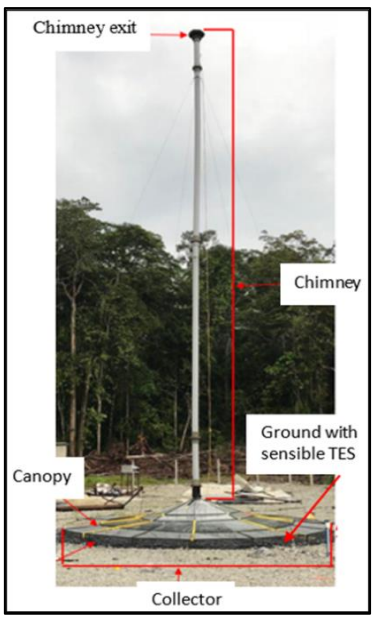


**Figure 1.** 15-m-height solar chimney power plant model

The SC model, shown in Figure 1, has a chimney with a 15-m height above the ground and a collector with a 6.6-m diameter. The chimney is made of a PVC pipe with a total of 14.35 mm long and 0.152 mm diameter installed above the central metal fixture of the collector. The chimney's friction losses are relatively low due to its short length. The system was investigated at two collectors' diameters, 4.9 and 6.6 m. The collector was made of metal frames supported by legs anchored to the ground and covered by a canopy made of Perspex sheets.

The collector has double slopes. The inner part has a 20° slope, and the outer part has a 5° slope. Black materials are more efficient for solar photothermic conversion. A 100-mm thick layer of black-painted pebbles covered the absorbing ground of the collector. The black-painted pebbles increase solar absorption and create higher heat flux inside the collector. Also, it operates as sensible thermal energy storage to store the energy during solar time and discharge it after sunset.

### 2.2 Measurements and measuring instruments

The measurements were performed at three different collector sizes, including Case-1 with a 4.9-m-diameter, Case-2 with a 6.6-m-diameter, and Case-3 with a 6.6-m-diameter + 1 m extra sensible TES outside the canopy.

The measured variables in this experiment are temperatures, air velocity, solar irradiation, and humidity. The measuring instrument used is the Extech Model 45160 3-in-1 Humidity, Temperature, and Airflow Meter. It could measure air velocity in a range of 0.4 to 30 m/s with 0.1 resolution and ±0.9% m/s accuracy. It has an accuracy of ±1.2°C for temperature measurement in the range of 0°C to 50°C. The data obtained could be displayed directly on the device's LCD screen. For the solar irradiance, a solarimeter KIMO-SL 200 model is used. Solar irradiation ranges from 1.0 to 1300 W/m², with a 5% measurement accuracy and an operating temperature range from -10 to 50°C. One of the essential parameters to be measured is the outlet air temperature at the top of the chimney. A K-type thermocouple probe is installed at the top of the chimney around 200 mm below the exit to avoid the inflow effect and mixing with the ambient air. The probe is connected to a digital Data logger brand GRAPHIC GL820.

### 2.3 Data acquisition strategy

The experimental work was started in early Oct. 2021 with preparation, instrument calibration, and preliminary runs for checking. The data acquisition commenced on 12 Nov. 2021. For each case, the experimental measurements were performed three days from 8:00 AM to 6:00 PM. Repeatability is important to reduce the uncertainty of measurements and possible system and human errors. Then, the average was considered for the presentation and discussion of results. The details of the experimented cases are shown in Table 1.

For each case, temperatures, velocities, and solar irradiance were recorded at each hour, starting from 8.00 AM till 6:00 PM. The temperature probe was placed at different points on the collector. The inlet temperature is measured at four locations of the canopy's circumferential and repeated many times at North, South, West, and East. The average of the four readings is considered for calculations and analysis. The measuring device typically used for incident solar radiation is a solarimeter that measures direct and diffuse combined solar radiation. The recorded data was clustered in an Excel file for further analysis.

### 2.4 Data interpretation

The selected data was able to characterize the SCPP performance and permit comparison between the investigated cases. The Performance Indicator (P.I.) is a parameter that represents the amount of increased air temperature of the generated air mass flow rate in the system. The P.I. is a highly

recommended parameter to compare various design and operational cases of solar updraft power.

$$P.I. = \dot{m} \times (T_{chimney,out} - T_{amb}) \quad (1)$$

The term ($T_{chimney,\ out} - T_{amb}$) represents the air temperature rise across the system, from the inlet to the ambient to the outlet at the top of the chimney. The mass flowrate is predicted using the measured velocity, $V_{chimney}$ at a plane 1.0 m above the chimney inlet to ensure fully developed flow, and the chimney cross-sectional area, as:

$$\dot{m} = \rho \times V_{chimney} \times A_{chimney} \quad (2)$$

**Table 1.** Details of the experimental cases

| Case | Dates of Experiments | Details of Configuration and Top View |
|---|---|---|
| Case-1 | 12, 13 and 14 Nov. 2021 | 4.9 m collector dia. 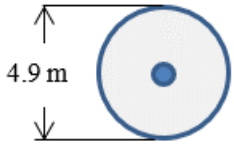  |
| Case-2 | 18, 19, and 20 Nov. 2021 | 6.6 collector dia. 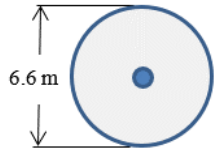  |
| Case-3 | 23, 24, and 25 Nov. 2021 | 6.6 + 2 m extended TES dia. 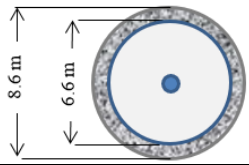  |

## 3. COMPUTATIONAL METHODOLOGY

The model's fluid dynamics prediction was achieved through computational modeling, simulation, and numerical solution of the mass, momentum, and energy conservation equation. The numerical solution was performed utilizing ANSYS Fluent software.

### 3.1 Computational model and assumptions

The experimental setup has been modeled in the computational fluid dynamic (CFD) simulation. The computational model with details is shown in Figure 2.

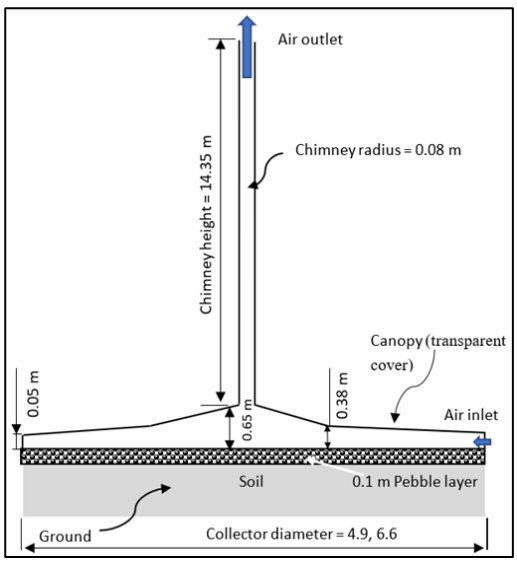


**Figure 2.** Computational model

The simulation was carried out assuming steady-state, turbulent, 2-D flow. The incompressible flow assumption is justified since the maximum Mach number is very small, < 0.1. The buoyancy effects were considered to occur due to temperature gradient, according to the Boussinesq criteria presented in Eq. (3). Air density change in the momentum equation is a function of temperature difference. This model treats density as a constant value in all solved equations except for the buoyancy term in the momentum equation. This model accounts for the full bouncy effect, where the density varies with temperature, and the flow is motivated by the force of gravity, which influences the change in density.

$$(\rho - \rho\_o\ )g \approx -\rho\_o\ \beta(T - T\_o\ )g$$
$$\rho = \rho_o(1 - \beta\Delta T) \quad (3)$$

Eq. (3) is valid for $\frac{\Delta\rho}{\rho_o} \leq 0.1$.

**Table 2.** Thermal and physical properties of the material for simulation

| Property | Materials | | |
|---|---|---|---|
| | Perspex (Canopy) | Black pebble (ground) | PVC Chimney |
| Absorption coefficient | 0.06 | 0.9 | 0.04 |
| Transmission coefficient | 0.92 | 0 | 0 |
| Density (kg/m$^3$) | 2700 | 2640 | 833 |
| Specific heat (J/kg·K) | 840 | 820 | 1170 |
| Thermal conductivity (W/m·K) | 0.78 | 1.73 | 0.19 |
| Emissivity | 0.9 | 0.9 | 0.91 |

The materials selected for the canopy were Perspex acrylic with 4-mm-thickness, with a transmission coefficient of 0.92. The medium selected for the absorbing surface was black-painted pebbles with an absorptivity of 0.9 and emissivity of 0.95 [12]. A summary of the material properties used in the simulation is provided in Table 2.

Creating a symmetry wall along the center of the SC allows a reduction of the physical size of the computational model, thus reducing the computing time. The boundary conditions for the model are presented in Figure 3. The inlet to the system is the edge of the domain parallel to the collector inlet, while the outlet is the edge of the domain above the chimney outlet. Both the inlet and outlet are set at zero-gauge pressure.

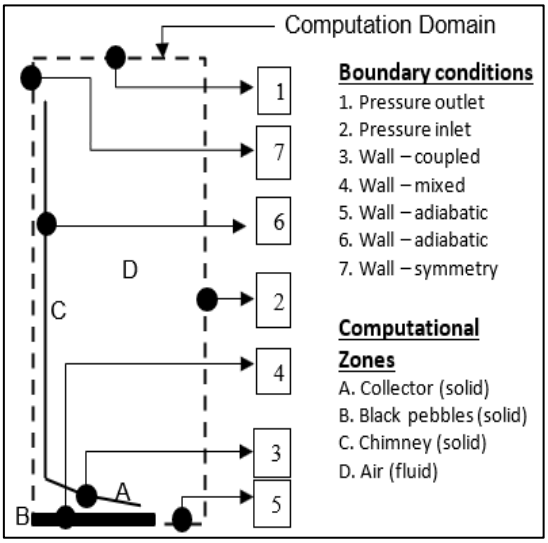


**Figure 3.** Computational domains and boundary conditions

### 3.2 Meshing and mesh independence check

The computational model, shown in Figure 2, was discretized using a structural grid. The grid near the walls was refined adaptively. Simulation results using different grid sizes and different strategies for grid refinement indicated that the selected grid was sufficiently fine to obtain grid-independent solutions. The final decision on the mesh and elements size is selected based on a difference of less than 1.0% in velocity measurements in the chimney when compared to a mesh model with a higher number of elements. The decided computational model is built with 111,884 elements and 112,108 nodes using quadrilateral elements. Figure 4 shows the meshed model at the collector region in ANSYS. Second-order upwind scheme was chosen for the convective terms.

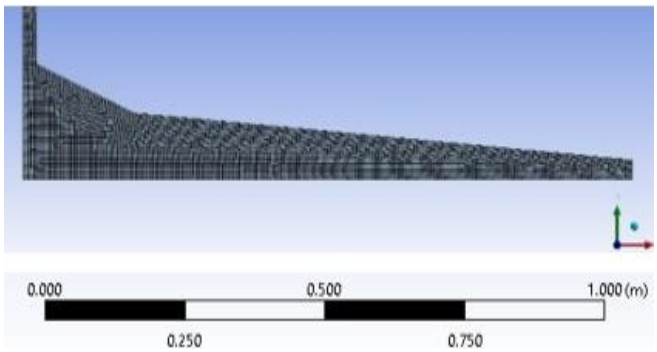


**Figure 4.** The mesh model in the collector region

### 3.3 Solution procedure

The collector thermal conditions were coupled with an internal emissivity of 0.9. The collector is treated as a semi-transparent wall, where the discrete ordinate (DO) model solves radiation heat transfer. The solar absorption by the collector was divided into two different computational zones. One zone is the ground under the collector, set as black-painted pebbles. The zone's temperature is 320 K, measured experimentally, with a heat transfer coefficient of 8 $W/m^2 \cdot K$. The second zone was outside the canopy diameter, the normal ground, which was set as an adiabatic wall.

The "SIMPLE" algorithm (Semi-Implicit Method for Pressure Linked Equations) was adopted to perform the numerical solutions of the governing equations. Heat transfer in the SCPP involves all three modes: conduction, convection, and radiation. Radiation heat transfer mainly occurs in the collector, covered by different types of semi-transparent material. The canopy material is nearly transparent for incident solar radiation but partly opaque for infrared radiation from the ground. The DO radiation model was adopted in the present simulations to solve the radiative transfer equation. It is the only model that can be used to model semi-transparent walls of various types. The DO model can compute non-grey radiation using a grey band model and works well across a full range of optical thicknesses. In the 2-D numerical simulation of the solar chimney, incident solar radiation on the ground through the semi-transparent collector is commonly treated as an internal heat source or heat flux [12].

## 4. RESULTS AND DISCUSSION

This section involves the presentation of the validation of the CFD simulation, the experimental results, and some simulation results.

### 4.1 Validation of the CFD procedure and results

The results for the velocity at the chimney base and the air temperature difference inside the system from the numerical simulation are compared against experimental data to validate the model. Table 3 shows the summary of the comparison of the results.

**Table 3.** Validation results by comparison of the measured and predicted velocities and the air temperature rise

| Parameter | Experiment | Simulation | Difference |
|---|---|---|---|
| Velocity at the chimney base | 1.256 m/s | 1.102 m/s | 12% |
| Air temperature rise, $\Delta T$ | 3.8 K | 4.1 K | 7.9% |

As the simulation is conducted based on constant ambient conditions, the data referred to from the experiment is taken at the closest values. Several parameters, like ambient wind and humidity, are not considered for the simulation. This coarse assumption may more or less influence the accuracy of the simulation results compared to the practical working conditions outside the SC. Still, it will not significantly influence the main objective of this paper. The model is accepted for further investigation based on the percentage difference between the experiment and simulation data.

### 4.2 Experimental results and analysis

Three different cases have been experimented with the same chimney of 15-m-height. Each case was repeated for three days, and the mean values were considered for the presentation and analysis of the results.

4.2.1 Analysis of case-1

In this case, the canopy has a 4.9 m diameter with the ground covered by matte black painted pebbles, as sensible TES. Figure 5 illustrates the system performance determined for three days of repeated measurements and the mean result and collector through the 3 days. The system performance increases as the air temperature increases due to the large amount of converted solar radiation. The maximum performance does not reach its maximum in the middle of the day, as experienced in most of the solar systems. The system performance keeps increasing and reaches a peak at around 2:00 PM. The reason is due to the type of ground that was converted by matte black painted pebbles. The maximum mean system performance indicator did not exceed 0.125 kg·K/s.

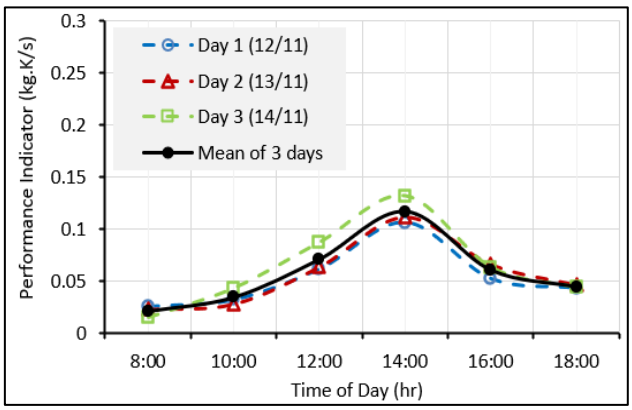


**Figure 5.** System performance for 3 days with 4.9 m canopy diameter (Case-1)

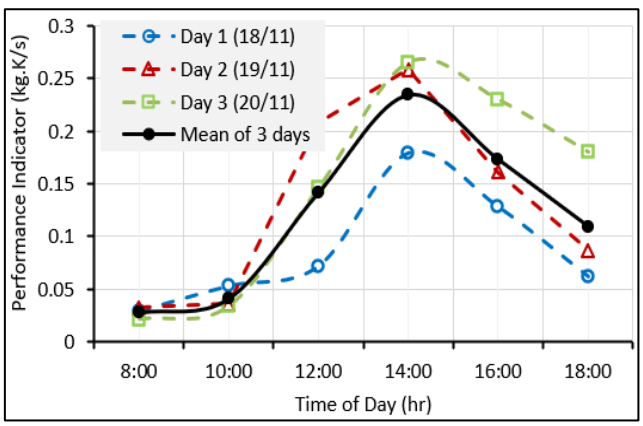


**Figure 6.** System performance through 3 days with a 6.6 m canopy diameter (Case-2)

4.2.2 Analysis of case-2

In this case, the canopy diameter was increased to 6.6-m-diameter with the ground covered by matte black painted pebbles. The inclination angle of the canopy after installing the frames around it is fixed to be 20° with respect to the horizontal surface. The measured inlet height was found to vary within a range of 100-120 mm due to the nature of the pebble layer. The system behavior is illustrated in Figure 6 in terms of the performance indicator. A similar trend could be observed in the system performance with time over the day, as in Case-1. However, the value much differ as there is a noticeable increase in the P.I. values. The maximum P.I. occurred at around 2:00 PM, like Case-1, but with almost double value, at 2.37 kg·K/s. This increase indicates the effectiveness of increased collector area on the SC performance. It could be noticed that the measurement data has a wider variation compared to Case-1, which indicates the necessity for repeated measurements of outdoor solar system investigation.

4.2.3 Analysis of case-3

This case has a canopy with a 6.6 m diameter, but the absorbing ground diameter was extended by an extra 2.0 m of black-painted pebbles surrounding the collector. The canopy does not cover the extended sensible TES. The pebble is just lying outside the canopy. This aims to realize the effect of heating the air outside the canopy to reduce the cost of canopy construction. However, the results of the three days of repeated measurements are shown in Figure 7. The system performance was considerably increased compared to Case-1 and Case-2. The peak performance, indicated by maximum P.I., occurred around 2:00 PM, similar to Case-1 and Case-2.

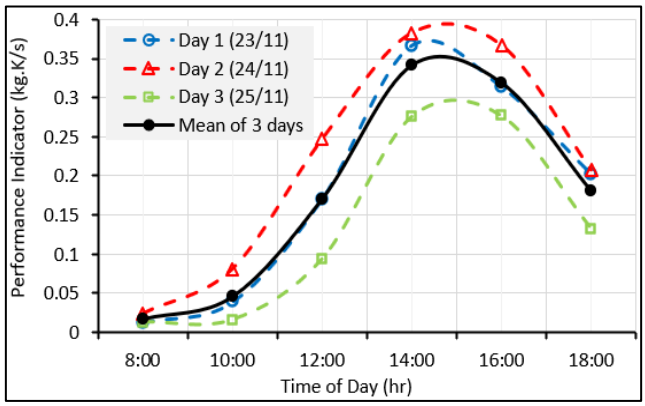


**Figure 7.** System performance through 3 days with a canopy of 6.6-dia. + 2.0-m-dia. extension of black-painted pebbles

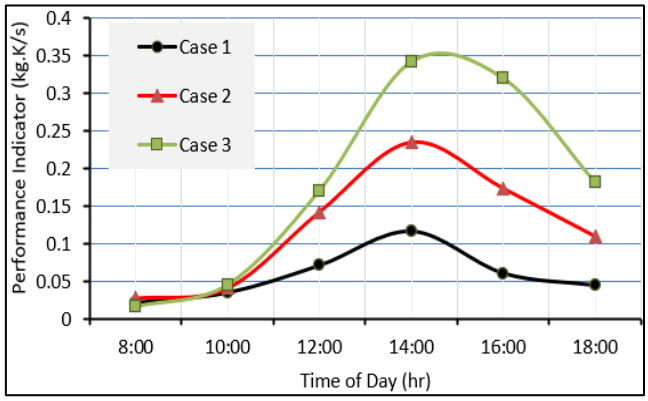


**Figure 8.** Comparison of the system performance between the three experimental cases

4.2.4 Comparison between the cases

Figure 8 illustrates the mean values of the system performance of the three experimented cases. The system performance in Case-3 is double that in Case-2. The pebble's

extension has significantly contributed to enhancing the system's performance. The mean values of the PI over the time 8:00 AM to 06:00 AM are 0.06, 0.12, and 0.18 for Case-1, Case-2, and Case-3, respectively.

Air particles are gaining heat by convection over the open area of the sensible TES. According to the physics of convection heat transfer, the particles are proposed to move up, but due to the suction phenomena at the covered part of the collector, the heated air particles in the outer region are moving to the internal passage of the collector, with a higher temperature than the ambient temperature. In spite of the fact that the investigated system is relatively small, a considerable enhancement without extra canopy diameter or extra chimney height has been achieved. This is an encouraging finding to reduce the system construction size and lower the costs of power production. On the other hand, it extends the SCPP production after sunset due to the heat discharging from stored energy in the pebbles to the flowing air inside the collector.

### 4.3 Numerical results

The predicted temperature distribution of air in the chimney is presented in Figure 9 and Figure 10 for all three cases at solar irradiance of 1000 W/m$^2$. Case-1 shows a maximum temperature of 316.2 K, a 13% temperature increase from the ambient temperature. As the collector diameter increased to 6.6 m in Case-2, the maximum air temperature predicted in the chimney is 317.50 K, which is a 17% increase from the ambient. With the addition of the extended ground medium in Case-3, the air temperature increase is 20%, with a maximum temperature of 318.6 K in the chimney.

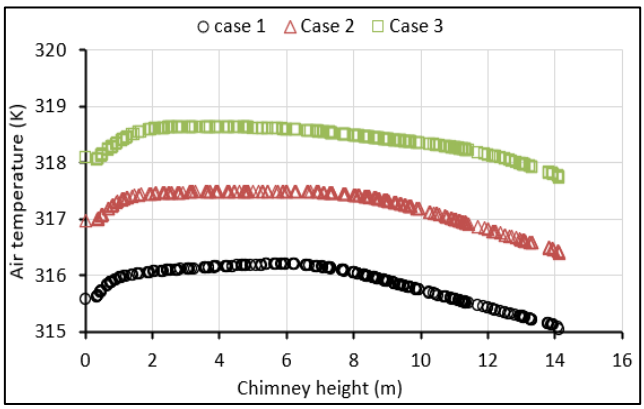


**Figure 9.** Predicted air temperature along the chimney centerline for three cases at 1000 W/m$^2$ solar irradiance

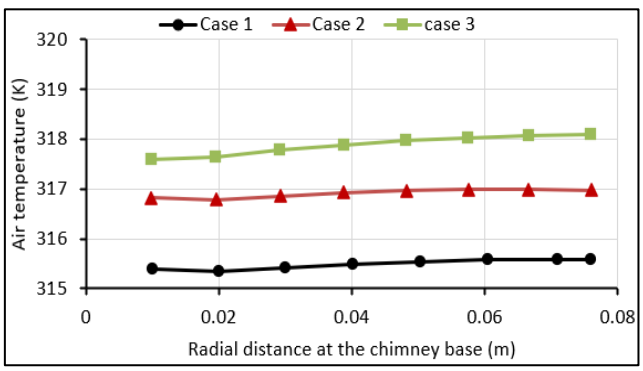


**Figure 10.** Predicted air temperature at the chimney base (radial position) for three cases at 1000 W/m$^2$ solar irradiance

Temperature results show an increase in air temperature near the chimney base and then a decrease for all simulated cases. Near the chimney base, the air is heated due to the metal structure at the central part of the model. This metal structure is painted black, and its temperature increases considerably, and sometimes it reaches above 90°C in the experimental model. The accumulated heat in the metal structure transfers thermal energy to the air at this portion, causing the air temperature to increase. However, above this metal structure, air starts losing thermal energy to the environment across the chimney wall, as the air temperature inside the chimney is higher than the ambient temperature.

The temperature distribution results are visualized in Figure 11, where the air temperature contours in the region between the collector and chimney show that the temperature is overall higher in Case-3. The effect of changing the diameter and adding the extended ground assembly has a positive impact on the overall temperature distribution throughout the SC domain. This is supported in Figure 11, which shows the air temperature contours at the collector inlet region. For Case-1 with the 4.9-m-diameter collector, the gap between the canopy inlet (periphery) and the ground is bigger, as per the experiment. This results in more heat losses to the surroundings, resulting in lower temperature gain. The smaller diameter also equals fewer greenhouse effects in the SC, compared to Case-2 with the 6.6-m-diameter collector.

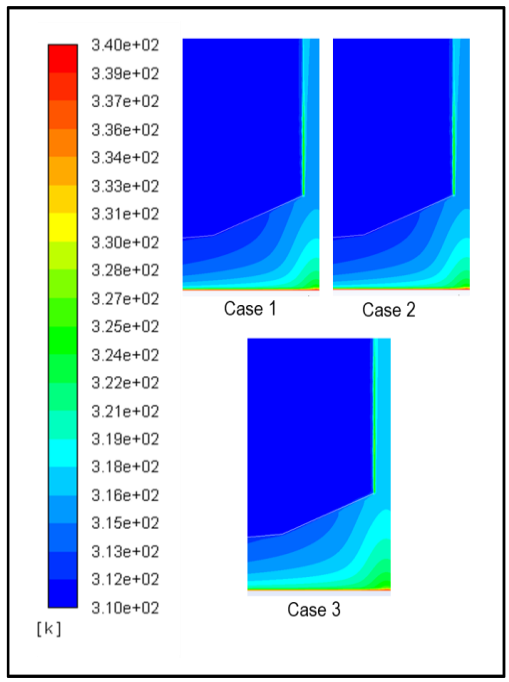


**Figure 11.** Contours of air temperature in the chimney base region for all cases at 1000 W/m$^2$ solar irradiance

Air velocity trends are predicted and presented in Figure 12 for all cases at solar irradiance of 1000 W/m$^2$. The results agree with the experimental velocity data at the chimney base, where the maximum velocity attained for each case is 1.129 m/s, 1.577 m/s, and 2.054 m/s, respectively. These values translate to an improvement of 30.2% in chimney velocity when the extended sensible TES is added to the SC computational domain when the collector diameter is kept constant. When the collector diameter increased from 4.9 m to 6.6 m, the velocity at the chimney increased over the tested range of the solar irradiation by 9%. Extending the sensible TES area by 2 m

extra diameter outside the canopy enhanced the system performance as the air velocity at the chimney base increased by 30.4% compared to Case-2 and 36.7% compared to Case-1.

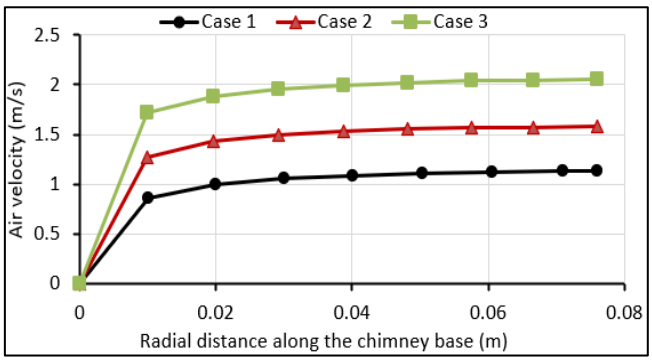


**Figure 12.** Predicted air velocity at the chimney base (radial position) for all cases at 1000 W/m$^2$ solar irradiance

Figure 13 visualizes the air velocity in the computational domain at the chimney base and collector inlet regions. The increased airflow seen in Case-2 and Case-3 results from the increased collector diameter (in both cases) and the addition of the extended sensible TES outside the collector in Case-3. In all simulated cases, the flow seems more uniform and streamlined near the surfaces of the collector, canopy, and ground. When the flow approaches the chimney base, a sort of mixing takes place, causing recirculation before entering the chimney. This may suggest that the connection between the chimney and the canopy should be more streamlined to smooth the flow entry to the chimney and avoid pressure losses due to circulation.

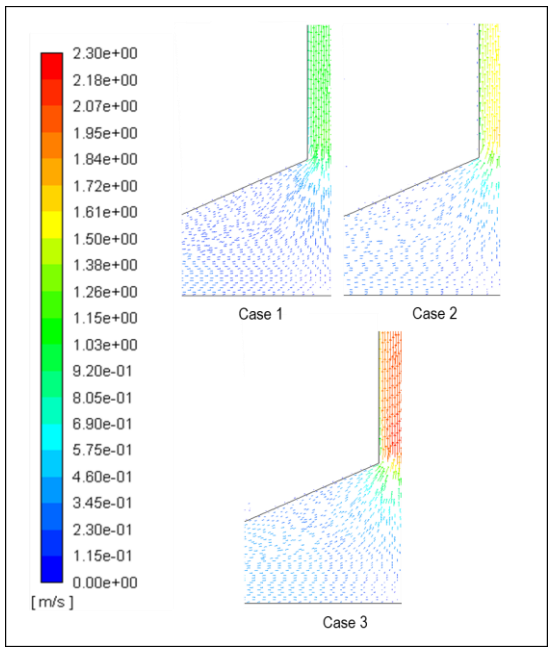


**Figure 13.** Air velocity vectors in the chimney base region for all cases at 1000 W/m$^2$ solar irradiance

A surge of air is visualized at the collector inlet in Case-2 and Case-3 is realized in the velocity vector of Figure 14. This corresponds to a low-pressure region at the collector inlet, as shown in Figure 15. The pressure is reduced in Case-2 and Case-3 compared to Case-1. The local increase in air temperature at the collector inlet region improves the inflow of air into the system, which results in high air velocity and low pressure in that region. The low-pressure region largely increases the velocity and the mass flow rate. As a result, the power in the air stream in the system increases in Case-2 and Case-3 due to the extension of the sensible TES outside the collector area.

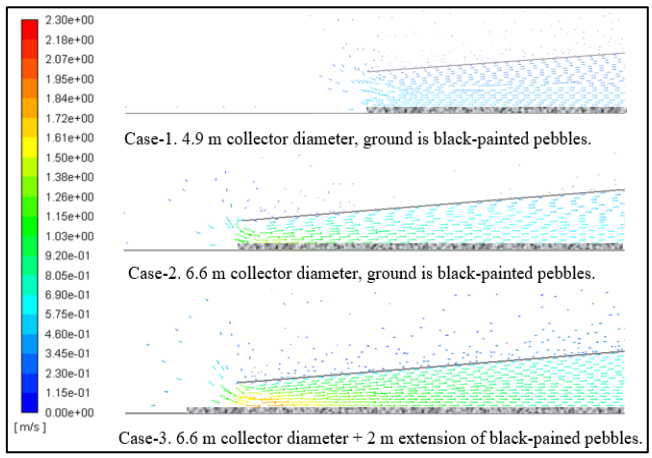


**Figure 14.** Air velocity vectors at the collector inlet region for all cases at 1000 W/m$^2$ solar irradiance

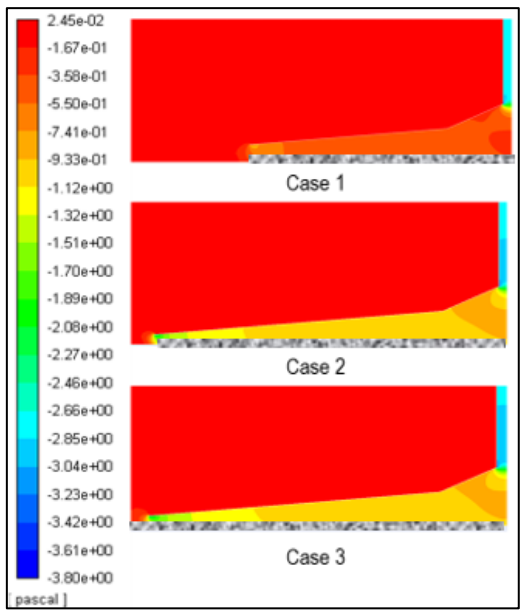


**Figure 15.** Contours of pressure at the collector inlet region for all cases at 1000 W/m$^2$ solar irradiance

## 5. CONCLUSION

An experimental model of a solar chimney with a 15-m height and three different collector configurations has been evaluated. The system is modelled computationally to allow visualization of the flow and heat transfer behavior at each experimented case. The work focused on the effect of added sensible TES on the absorbing ground of the collector. The extended layer of black-painted pebbles outside the canopy has significantly enhanced the performance of the solar chimney by 100% compared to the case without extended TES. The simulation results are compatible with the experimental results. The adopted simulation could be extended to predict

the influence of the extended sensible TES with various diameters beyond the canopy diameter.

## ACKNOWLEDGMENT

The authors acknowledge Universiti Teknologi PETRONAS for the support in conducting the research and producing this paper using the facilities in the solar research site.

## REFERENCES

[1] Chikere, A.O, Al-Kayiem, H.H., Karim. Z.A.A. (2011). Review on the enhancement techniques and introduction of an alternate enhancement technique of solar chimney power plant. Journal of Applied Sciences, 11: 1877-1884. https://doi.org/10.3923/jas.2011.1877.1884

[2] Al-Kayiem, H.H., Chikere A.O. (2016). Historic and recent progress in solar chimney power plant enhancing technologies. Renewable and Sustainable Energy Reviews, 58: 1269-1292. https://doi.org/10.1016/j.rser.2015.12.331

[3] Kasaeiana, A.B., Molanaa, K.S., Wen., R.D. (2017). A review on solar chimney systems. Renewable and Sustainable Energy Reviews, 67: 954-987. https://doi.org/10.1016/j.rser.2016.09.081

[4] Ahmed, O.K., Algburi, S., Ali, Z.H., Ahmed, A.K., Shubat, H.N. (2022). Hybrid solar chimneys: A comprehensive review. Energy Reports, 8: 438-460. https://doi.org/10.1016/j.egyr.2021.12.007

[5] Cuce, E., Cuce, P.M., Carlucci, S., Sen, H., Sudhakar, K., Hasanuzzaman, M., Daneshazarian, R. (2022). Solar chimney power plants: A review of the concepts, designs and performances. Sustainability, 14(3): 1450. https://doi.org/10.3390/su14031450

[6] Al-Azawiey, S.S., Al-Kayiem, H.H., Hassan, S. (2017). On the influence of collector size on the solar chimneys performance. In MATEC Web of Conferences, 131: 02011. https://doi.org/10.1051/matecconf/201713102011

[7] Al-Azawiey, S.S., Al-Kayiem, H.H., Hassan, S. (2016). Investigation on the influence of collector height on the performance of solar chimney power plant. ARPN Journal of Engineering and Applied Sciences, 11(20): 12197-12201.

[8] Zhou, X., Yang, J., Xiao, B., Hou, G. (2007). Experimental study of temperature field in a solar chimney power setup. Applied Thermal Engineering 27(11-12): 2044-2050. https://doi.org/10.1016/j.applthermaleng.2006.12.007

[9] Kasaeian, A.B., Heidari, E., Vatan, S.N. (2011). Experimental investigation of climatic effects on the efficiency of a solar chimney pilot power plant. Renewable Sustainable Energy Reviews, 15: 5202-5206. https://doi.org/10.1016/j.rser.2011.04.019

[10] Lal, S., Kaushik, S.C., Hans, R. (2016). Experimental investigation and CFD simulation studies of a laboratory scale solar chimney for power generation. Sustainable Energy Technologies and Assessments, 13: 13-22. https://doi.org/10.1016/j.seta.2015.11.005

[11] Rao. K.R. (1984). Energy conservation possibilities through building design and passive cooling techniques in warm climates. Energy Developments: New Forms, Renewables, Conservation, In Proceedings of ENERGEX, Saskatchewan, Canada, 84: 433-439. https://doi.org/10.1016/B978-0-08-025407-4.50080-6

[12] Al-Azawiey, S.S., Hassan, S. (2016). Heat absorption properties of ground material for solar chimney power plants. International Journal of Energy Production and Management, 1(4): 403-418. https://doi.org/10.2495/EQ-V1-N4-403-418

## NOMENCLATURE

| Symbol | Definition |
|---|---|
| $A_{chimney}$ | Cross-sectional area of the chimney ($m^2$) |
| $\dot{m}$ | Mass flow rate (kg/s) |
| $T_{chimney.\ out}$ | Exit air temperature at top of the chimney (°C) |
| $T_{amb.}$ | Ambient temperature (°C) |
| $T_o$ | Reference air temperature (°C) |
| $V_{chimney}$ | Airflow velocity at chimney base (m/s) |

### Greek symbols

| | |
|---|---|
| $\rho$, $\rho_o$ | Air density, Reference density ($kg/m^3$) |
| $\beta$ | Volumetric coefficient of thermal expansion |

### Acronyms

| | |
|---|---|
| CFD | Computational Fluid Dynamics |
| DO | Discrete Ordinate radiation model in ANSYS |
| P.I. | Performance indicator (kg·K/s) |
| PVC | Polyvinyl Chloride |
| SIMPLE | Semi-Implicit Method for Pressure Linked Equations |
| SC | Solar chimney |
| SCPP | Solar chimney power plant |
| TES | Thermal energy storage |